Supplementary Data

Hydrolysis of the Fluorogenic Peptides

suc-LLVY-MCA was utilized as the standard peptide to assess the chymotrypsin-like activity of the core. 20SPT (0.5–3 μg) was incubated at 37°C in 20 mM Tris/HCl, pH 7.5 buffer. Incubation was initiated by the addition of 100 μM of suc-LLVY-AMC. Fluorescence emission was recorded at 430 nm (excitation at 365 nm). The measurement of 20SPT activity using the fluoropeptide suc-LLVY-AMC was established by generating a curve at increasing proteasomal concentrations. We monitored the fluorescence signal every 2 min for 45 min and used the data in the linear range. The results were compared to the fluoroprobe (AMC) standard curve to ensure that the data fit into the initial rates in which no more than 5% of the substrate is consumed.

Two-dimensional Gel Electrophoresis (2-DE) and In-gel Digestion

The His-tagged 20SPT was isolated as described in Materials and Methods. Cell protein extraction and proteasome purification were carried out in 50 mM Tris-HCl pH 7.5 buffer containing 500 mM NaCl, 5 mM $MgCl_2$, and 20 mM imidazole. Final preparations were passed through a PD10-desalting column (GE Healthcare) and eluted in 10 mM Tris-HCl pH 7.5 buffer. Samples were concentrated in a 100 kDa cut-off microcon spin filter (Millipore) to achieve desired concentration (2–3 μg/μL). Prior to IPG strips rehydration, final preparations (100–150 μg) were mixed up with thiourea rehydration solution (7 M urea, 2 M thiourea, 2 % [w/v] CHAPS, 0.5 % IPG buffer, pH 4–7, 0.002% bromophenol blue) to a final volume of 340 μL. Eighteen-centimeter IPG strips (pH 4–7) were rehydrated for 16 h at room temperature. IEF was conducted in a IPGphor 3 IEF system (GE Healthcare) according to the voltage gradient table below:

Mode	*Voltage*	*Vh accumulation*	*Time*	
1. Step	500 V	500	~1 h	
2. Gradient	1000 V	800	~1 h	
3. Gradient	10,000 V	16,500	~3 h	
4. Step	10,000 V	13,700	~1.5 h	Total 31,500 V/h

The second dimension was performed in 12.5% SDS-PAGE, with the vertical Ettan-DALTsix Electrophoresis System (GE Healthcare). The gels were run at constant current (15 mA) for 45 min. Next, the current was increased to 45 mA and kept constant until the end of the run. Protein spots were visualized by Coomassie Brilliant Blue R-250 staining. Selected spots were excised and destained. Proteins were in-gel digested with Trypsin Gold (Promega, Mass Spectrometry Grade), according to the protocol provided by Promega.

MALDI–TOF-MS Fingerprinting of the Proteasome Subunits

The mass spectrometry identifications of the proteasomal subunits isolated by 2-DE were performed using an Ettan MALDI-TOF system (Amersham Biosciences). Analyses of the tryptic digests of each spot were performed in reflectron mode with positive ionization at an acceleration voltage of 20 kV. The samples for MS analysis were spotted onto a MALDI slide, dried and covered with α-cyano-4-hydroxycinnamic acid (CHCA, saturated with 50% acetonitrile, 0.1% trifluoroacetic acid). The samples were analyzed by the Ettan Maldi Software and the final spectrum contained the sum of 200 accumulated spectra. For accessing the quality of the mass list, samples were applied in duplicate and utilized to confirm the presence of a given mass. Extracted mass measurements contained a signal to noise ratio higher than 3 and spectra resolution from 5000 to 8000 to assess monoisotopic distribution. The final spectrum contained the sum of the accumulated 200 spectra. The equipment was previously calibrated with standard peptides (Angio II $[M + H]^+$ 1046.54 and P14R $[M + H]^+$ 1533.86). The peptide mass fingerprint analysis was performed using the Mascot Server 2.2 software (Matrix Science, UK), and the search parameters were: SwissProt 51.6 database, *Saccharomyces cerevisiae* taxon, trypsin enzyme, methionine oxidation as variable modification, peptide charge state 1^+, one missed cleavage, and peptide mass tolerance of 0.25 Da. When present, masses of known contaminants (human keratin and trypsin autolysis peptides) were removed from the analysis.

SAXS Analysis of Proteasomal Redox Forms

The measured scattering data of both nPT-SG and PT-SH samples are shown in Supplementary Fig. S6. The scattering intensity is displayed as a function of q ($q = 4\pi \sin\theta/\lambda$, where λ is the radiation wavelength and 2θ is the scattering angle), the modulus of the reciprocal space momentum transfer vector. As the first analysis, we performed an independent modeling approach, using the indirect Fourier transformation (IFT) introduced by Glatter (2) in a slightly different implementation (10, 14). From this calculation, it is possible to obtain the pair distance distribution curve p(r) which provides real space information of particles in solution.

For both samples, the IFT fit provided the indication that the particles have an elongated conformation with maximum dimension of 230 Å (nPT-SG) and 200 Å (PT-SH). Also, the nPT-SG radius of gyration obtained was 65 ± 2 Å and 62 ± 1 Å in the case of PT-SH samples. The decreased radius of gyration might be explained by the differences in the p(r) curves. In p(r) curves from cylindrical particles, the point of inflexion after the maximum of the curve is a rough indication of the particle diameter. This indicates that 20SPT deglutathiolation induced a decrease on the particle diameter.

In order to go one step further on the data modeling, data was adjusted using a form factor of a hollow cylinder, with outer radius R_{out}, inner radius R_{in}, and length L. The form factor used in the modeling is given by

$$I_1(q) = \int_0^{\pi/2} \left[\frac{V(R_{out}) F_{cyl}(q, R_{out}) \exp\left(-\frac{q^2\sigma^2}{2} \right) - V(R_{in}) F_{cyl}(q, R_{in})}{V(R_{out}) - V(R_{in})} \right]^2 \sin \alpha d\alpha$$

Where,

$$F_{cyl}(R, L, \alpha) = \frac{2J_1(qR \sin \alpha)}{qR \sin \alpha} \frac{\sin(qL \cos \alpha/2)}{qL \cos \alpha/2}$$

$$V(R) = \pi R^2 L$$

The Gaussian term $\exp(-q^2\sigma^2/2)$ provides a diffuse interface for the outer diameter of the cylinder. As will be shown below, it can be seen from the known 3D structure of yeast proteasome (pdb entry 3d29) the presence of several helices sticking out of the surface and therefore this diffuse interface might mimic this effect. The fit is shown in Supplementary Fig. S7.

The modeling using the theoretical form factor supported the results obtained by the IFT analysis indicating that proteasomal deglutathiolation decreases the outer diameter of the cylinder. Also, the fitting procedure indicated that the inner radius of the PT-SH presents an important decrease, almost closing completely. These results strongly indicate that proteasomal deglutathiolation induces conformational changes that decrease outer and inner radius closing the gate.

As an additional step of the data analysis, the scattering data were compared with available atomic resolution structure (6) (pdb entry 3d29). Two views of the protein structure are shown in Supplementary Figs. S8 and S9. The figures were generated using software MolMol (8) and Massha (7).

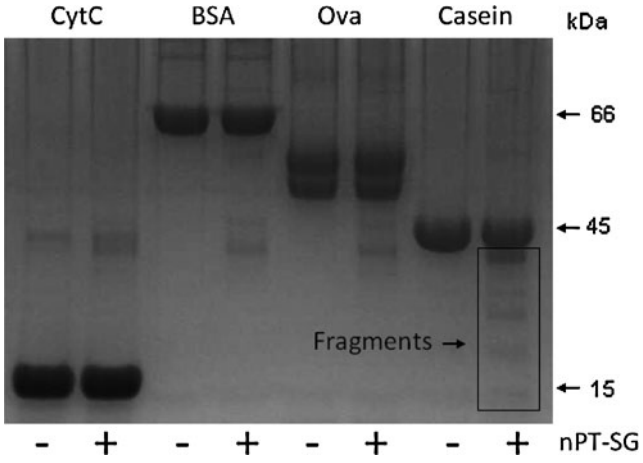

SUPPLEMENTARY FIG. S1. Protein incubation with nPT-SG. The image shown is a representative SDS-PAGE of 15-μg protein samples incubated for 3 h at 30°C in the presence (+) or absence (−) of 5 μg of nPT-SG: cytochrome c (CytC), non-oxidized albumin (BSA), and ovalbumin (Ova). Casein, utilized as a model of unstructured protein, was incubated for 10 min with the nPT-SG. After incubation, the samples were filtered through YM-100 microfilters (Millipore) to remove the 20SPT, and the filtrates were applied to a 15% SDS-PAGE.

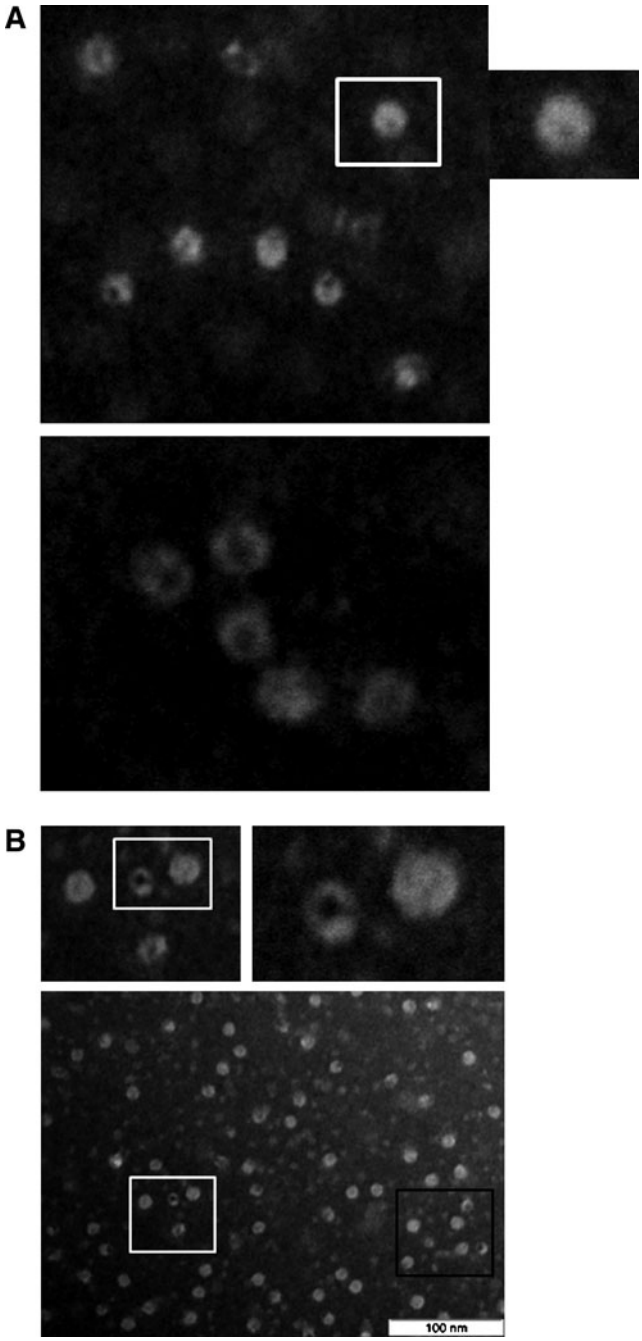

SUPPLEMENTARY FIG. S2. 20S proteasomal gating. (A) Representative images obtained by transmission electron microscopy of nPT-SG exhibiting both closed and open conformation. **(B)** PT-SH samples analyzed immediately after treatment with 20 mM DTT for 30 min followed by washing procedure to eliminate DTT, as described in Materials and Methods. Combined conformations (open and closed) are highlighted by squares and amplified, as seen.

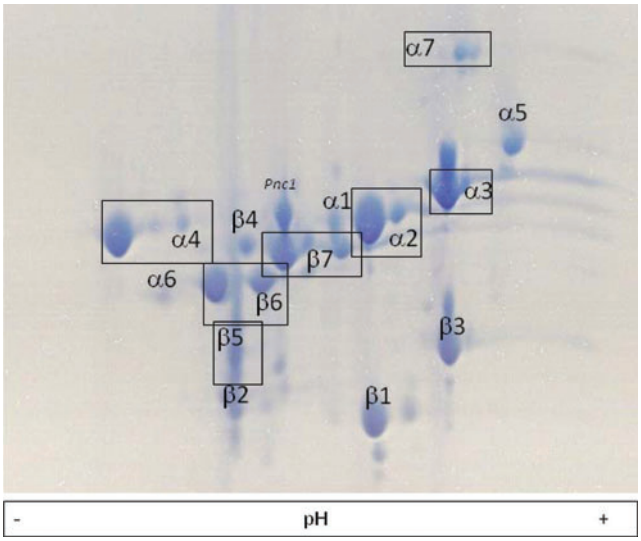

SUPPLEMENTARY FIG. S3. Two-dimensional electrophoresis of the 20S proteasome (20SPT) from *S. cerevisiae*. The 20SPT (150 μg) purified from yeast *S. cerevisiae* was isoelectric focused on IPG strips (pH range 4–7) followed by 12.5% SDS-PAGE and Coomassie Brilliant Blue G-250 staining. The labeled subunits were identified by Maldi-TOF fingerprinting analysis after in-gel tryptic digestion using Mascot software (Matrix Science) as the search engine. The nicotinamidase Pnc1 was co-purified and identified by MS fingerprinting.

The structure shown in Supplementary Fig. S8 has a cylinder-like shape and the overall dimensions can be extracted from the panel shown in Supplementary Fig. S10: cylinder height = 150 Å, outer diameter = 110 Å, and inner diameter = 50 Å.

Taking the comparison of the theoretical intensity calculated from structure shown in Supplementary Fig. S8 together with experimental data, we obtained the fit given in Supplementary Fig. S10. The theoretical intensity from the atomic coordinates was performed using program CRYSOL (16). As can be seen from the fit, the proteasome is reasonably described by the atomic resolution model, while there is a larger discrepancy in the data obtained from PT-SH samples.

The SAXS data indicated that proteasome samples in solution can be well described as short hollow cylinders. However, dimensions and characteristics of the 20SPT redox forms are remarkably different. The nPT-SG can be understood as a hollow cylinder in a reasonable agreement with the known atomic resolution structure of the proteasome. On the other hand, the PT-SH presents smaller cross section, indicating decreased outer radius. Also, the modeling indicated that the internal hole was almost completely closed after DTT treatment. The change in structure was also confirmed by comparison with the known atomic resolution structure discussed above.

These results are in agreement with the TEM data also presented in this work for both proteasomal redox conditions.

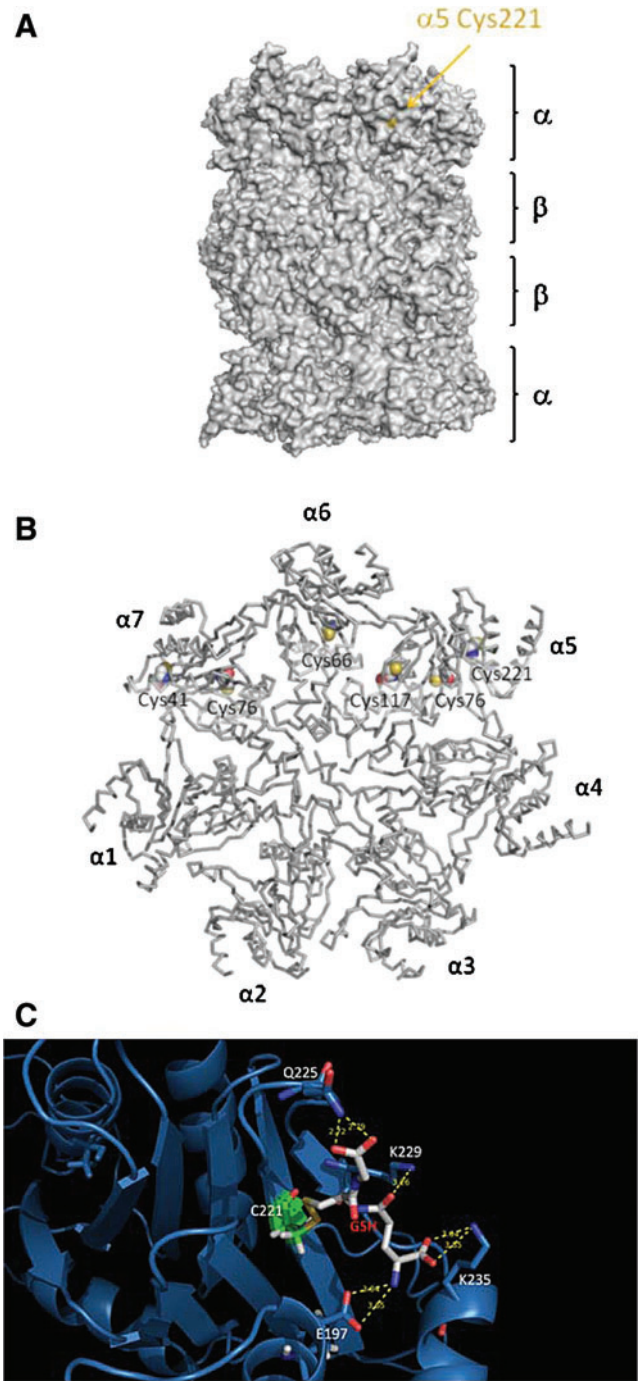

SUPPLEMENTARY FIG. S4. S-glutathiolated Cys residues in the 20SPT. (A) The sulfur atom of all S-glutathiolated residues is highlighted in yellow, indicating α5Cys221 solvent accessibility. **(B)** Proteasomal α ring highlighting S-glutathiolated Cys residues identified through LC-ESI-Q-TOF analyses. Cys221 and Cys76 in the α5 subunit were found glutathiolated in nPT-SG samples; the other Cys residues shown were found glutathiolated after the 10 mM GSH treatment of same samples. **(C)** An additional view of glutathione docking in the vicinity of α5Cys221 (green) modeled by Gold 4.1–Protein-Ligand Docking (Cambridge Crystallographic Data Centre). The proteasome is shown by cartoon representation, and glutathione is indicated by white sticks emphasizing the solvent accessibility of the protein thiol group (yellow). Proteasomal residues interacting with GSH-charged groups are shown as blue sticks. Distances between GSH-charged groups and lateral chains of proteasomal amino acids are also shown (Å).

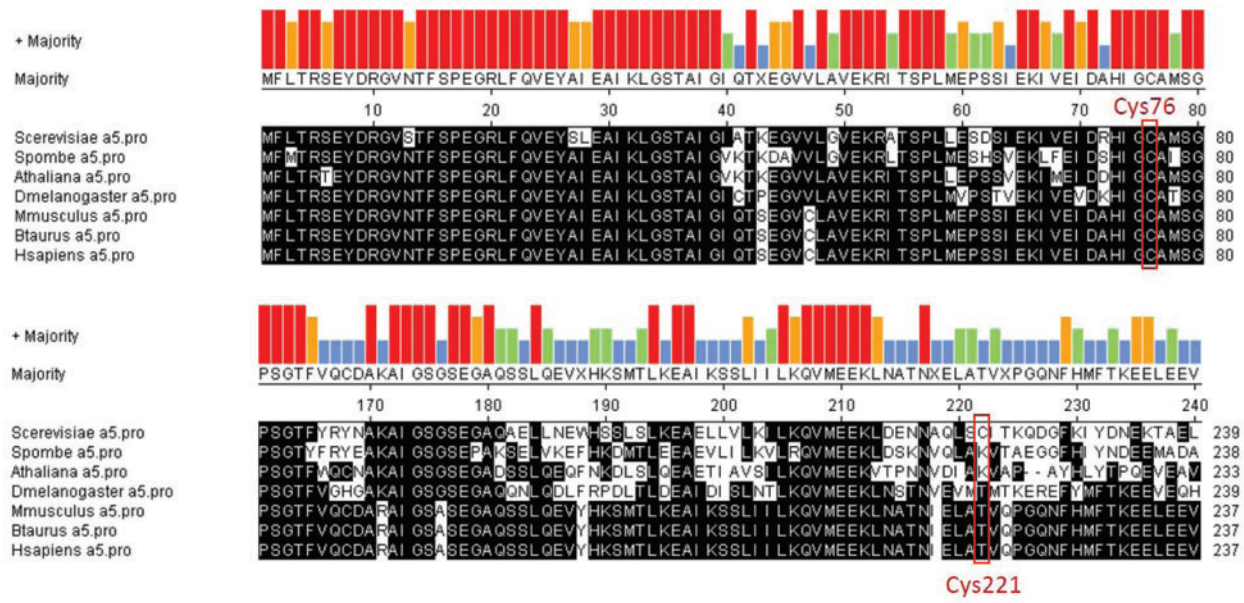


```
Btaurus_a5              MFLTRSEYDRGVNTFSPEGRLFQVEYAIEAIKLGSTAIGIQTSEGVCLAVEKRITSPLME 60
Hsapiens_a5             MFLTRSEYDRGVNTFSPEGRLFQVEYAIEAIKLASTAIGIQTSEGVCLAVEKRITSPLME 60
Mmusculus_a5            MFLTRSEYDRGVNTFSPEGRLFQVEYAIEAIKLGSTAIGIQTSEGVCLAVEKRITSPLME 60
Dmelanogaster_a5        MFLTRSEYDRGVNTFSPEGRLFQVEYAIEAIKLGSTAIGICTPEGVVLAVEKRITSPLMV 60
Athaliana_a5            MFLTRTEYDRGVNTFSPEGRLFQVEYAIEAIKLGSTAIGVKTKEGVVLAVEKRITSPLLE 60
Scerevisiae_Pup2        MFLTRSEYDRGVSTFSPEGRLFQVEYSLEAIKLGSTAIGIATKEGVVLGVEKRATSPLLE 60
Spombe_a5               MFMTRSEYDRGVNTFSPEGRLFQVEYAIEAIKLGSTAIGVKTKDAVVLGVEKRLTSPLME 60
                        **:**:******.*************::*****.*****: * :.* *.**** ****:
                                    Cys76
Btaurus_a5              PSSIEKIVEIDAHIGCAMSGLIADAKTLIDKARVETQNHWFTYNETMTVESVTQAVSNLA 120
Hsapiens_a5             PSSIEKIVEIDAHIGCAMSGLIADAKTLIDKARVETQNHWFTYNETMTVESVTQAVSNLA 120
Mmusculus_a5            PSSIEKIVEIDAHIGCAMSGLIADAKTLIDKARVETQNHWFTYNETMTVESVTQAVSNLA 120
Dmelanogaster_a5        PSTVEKIVEVDKHIGCATSGLMADARTLIERARVECQNHWFVYNERMSIESCAQAVSTLA 120
Athaliana_a5            PSSVEKIMEIDDHIGCAMSGLIADARTLVEHARVETQNHRFSYGEPMTVESTTQALCDLA 120
Scerevisiae_Pup2        SDSIEKIVEIDRHIGCAMSGLTADARSMIEHARTAAVTHNLYYDEDINVESLTQSVCDLA 120
Spombe_a5               SHSVEKLFEIDSHIGCAISGLTADARTIIEHARVQTQNHRFTYDEPQGIESTTQSICDLA 120
                        . ::**:.*:* ***** *** ***:::::::**.   .* : *.*   :** :*::. **

Btaurus_a5              LQFGEE-DAD-PGAMSRPFGVALLFGGVD-EKGPQLFHMDPSGTFVQCDARAIGSASEGA 177
Hsapiens_a5             LQFGEE-DAD-PGAMSRPFGVALLFGGVD-EKGPQLFHMDPSGTFVQCDARAIGSASEGA 177
Mmusculus_a5            LQFGEE-DAD-PGAMSRPFGVALLFGGVD-EKGPQLFHMDPSGTFVQCDARAIGSASEGA 177
Dmelanogaster_a5        IQFGDSGDSDGAAAMSRPFGVAILFAGIE-AGQPQLWHMDPSGTFVGHGAKAIGSGSEGA 179
Athaliana_a5            LRFGEG-EEE---SMSRPFGVSLLIAGHD-ENGPSLYYTDPSGTFWQCNAKAIGSGSEGA 175
Scerevisiae_Pup2        LRFGEGASGE-ERLMSRPFGVALLIAGHDADDGYQLFHAEPSGTFYRYNAKAIGSGSEGA 179
Spombe_a5               LRFGEGEDGE-ERIMSRPFGVALLIAGID-EHGPQLYHSEPSGTYFRYEAKAIGSGSEPA 178
                        ::**:  . :    *******::*:.* :     .*:: :****:    *:****.** *

                                                        Cys221
Btaurus_a5              QSSLQEVYHKSMTLKEAIKSSLIILKQVMEEKLNATNIELATVQPGQNFHMFTKEELEEV 237
Hsapiens_a5             QSSLQEVYHKSMTLKEAIKSSLIILKQVMEEKLNATNIELATVQPGQNFHMFTKEELEEV 237
Mmusculus_a5            QSSLQEVYHKSMTLKEAIKSSLIILKQVMEEKLNATNIELATVQPGQNFHMFTKEELEEV 237
Dmelanogaster_a5        QQNLQDLFRPDLTLDEAIDISLNTLKQVMEEKLNSTNVEVMTMTKEREFYMFTKEEVEQH 239
Athaliana_a5            DSSLQEQFNKDLSLQEAETIAVSILKQVMEEKVTPNNVDIAKVAP--AYHLYTPQEVEAV 233
Scerevisiae_Pup2        QAELLNEWHSSLTLKEAELLVLKILKQVMEEKLDENNAQLSCITKQDGFKIYDNEKTAEL 239
Spombe_a5               KSELVKEFHKDMTLEEAEVLILKVLRQVMEEKLDSKNVQLAKVTAEGGFHIYNDEEMADA 238
                        . .* . :. .::*.**    :  *:******:  .* ::  :     : ::  ::

Btaurus_a5              IKDI---------------- 241
Hsapiens_a5             IKDI---------------- 241
Mmusculus_a5            IKDI---------------- 241
Dmelanogaster_a5        IKNIA--------------- 244
```

SUPPLEMENTARY FIG. S5. Alignments of the primary sequences of the α5 and α7 20SPT subunits α5 (continued→)

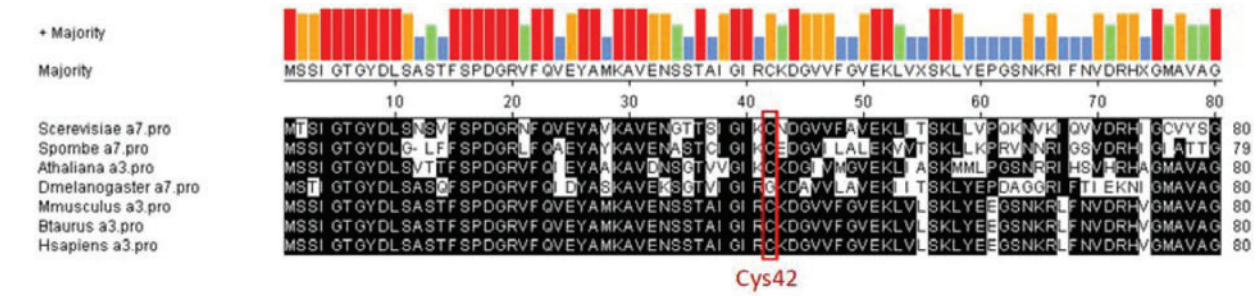


```
                                                    Cys42
Btaurus_a3              MSSIGTGYDLSASTFSPDGRVFQVEYAMKAVENSSTAIGIRCKDGVVFGVEKLVLSKLYE 60
Hsapiens_a3             MSSIGTGYDLSASTFSPDGRVFQVEYAMKAVENSSTAIGIRCKDGVVFGVEKLVLSKLYE 60
Mmusculus_a3            MSSIGTGYDLSASTFSPDGRVFQVEYAMKAVENSSTAIGIRCKDGVVFGVEKLVLSKLYE 60
Dmelanogaster_a7        MSTIGTGYDLSASQFSPDGRVFQIDYASKAVEKSGTVIGIRGKDAVVLAVEKIITSKLYE 60
Athaliana_a3            MSSIGTGYDLSVTTFSPDGRVFQIEYAAKAVDNSGTVVGIKCKDGIVMGVEKLIASKMML 60
Scerevisiae_Pre10       MTSIGTGYDLSNSVFSPDGRNFQVEYAVKAVENGTTSIGIKCNDGVVFAVEKLITSKLLV 60
Spombe_a7               MSSIGTGYDLG-LFFSPDGRLFQAEYAYKAVENASTCIGIKCEDGVILALEKVVTSKLLK 59
                        *::*******.   ****** ** :** ***::. * :**: :*.::::.**:: **:

Btaurus_a3              EGSNKRLFNVDRHVGMAVAGLLADARSLADIAREEASNFRSNFGYNIPLKHLADRVAMYV 120
Hsapiens_a3             EGSNKRLFNVDRHVGMAVAGLLADARSLADMAREEASNFRSNFGYNIPLKHLADRVAMYV 120
Mmusculus_a3            EGSNKRLFNVDRHVGMAVAGLLADARSLADIAREEASNFRSNFGYNIPLKHLADRVAMYV 120
Dmelanogaster_a7        PDAGGRIFTIEKNIGMAVAGLVADGNFVADIARQEAANYRQQFEQAIPLKHLCHRVAGYV 120
Athaliana_a3            PGSNRRIHSVHRHAGMAVAGLAADGRQIVARAKSEARSYESVYGDAVPVKELSERVASYV 120
Scerevisiae_Pre10       PQKNVKIQVVDRHIGCVYSGLIPDGRHLVNRGREEAASFKKLYKTPIPIPAFADRLGQYV 120
Spombe_a7               PRVNNRIGSVDRHIGIATTGFIPDGQHIVKRARDEATSWRDNYGSPIPGTVIADRLGNYV 119
                           . ::  :.:: * . :*: .*.. :.  .:.** .:.. :   :*   :..*:. **

Btaurus_a3              HAYTLYSAVRPFGCSFMLGSYSVNDGAQLYMIDPSGVSYGYWGCAIGKARQAAKTEIEKL 180
Hsapiens_a3             HAYTLYSAVRPFGCSFMLGSYSVNDGAQLYMIDPSGVSYGYWGCAIGKARQAAKTEIEKL 180
Mmusculus_a3            HAYTLYSAVRPFGCSFMLGSYSANDGAQLYMIDPSGVSYGYWGCAIGKARQAAKTEIEKL 180
Dmelanogaster_a7        HAYTLYSAVRPFGLSIILASWDEVEGPQLYKIEPSGSSFGYFACASGKAKQLAKTEMEKL 180
Athaliana_a3            HLCTLYWWLRPFGCGVILGGYDR-DGPQLYMIEPSGISYRYFGAAIGKGKQAAKTEIEKL 179
Scerevisiae_Pre10       QAHTLYNSVRPFGVSTIFGGVDK-NGAHLYMLEPSGSYWGYKGAATGKGRQSAKAELEKL 179
Spombe_a7               QLFTCYSSVRPFGVMSFVATYDS-EGPHLYMVEPNGVYWGYNGAAAGKGRQVARNELEKL 178
                        :  * *  :****   :..  .  :*.:** ::*.*  : * ..* **.:* *: *:***

Btaurus_a3              QMK---EMTCRDVVKEVAKIIYIVHDEVKDKAFELELSWVGE-ITNGRHEIVPKDVREEA 236
Hsapiens_a3             QMK---EMTCRDIVKEVAKIIYIVHDEVKDKAFELELSWVGE-LTNGRHEIVPKDIREEA 236
Mmusculus_a3            QMK---EMTCRDVVKEVAKIIYIVHDEVKDKAFELELSWVGE-LTKGRHEIVPKDIREEA 236
Dmelanogaster_a7        KM----DMRTDELVESAGEIIYKVHDELKDKDFRFEMGLVGR-VTGGLHLINPSELTEKA 235
Athaliana_a3            NLS---EMTCKEGVIEVAKIIYKLHDEAKDKAFELEMSWICE-ESKREHQKVPDDLLEEA 235
Scerevisiae_Pre10       VDHHPEGLSAREAVKQAAKIIYLAHEDNKEKDFELEISWCSLSETNGLHKFVKGDLLQEA 239
Spombe_a7               N---FSSLKMKDAVKEAARILYATHDEENNKEHEIEMTWVGV-ETNGIHTPVPDELLQEA 234
                              :   : * ....*:*  *:: ::* ..:*:       :   *     :: ::*

Btaurus_a3              EKYAKESLKEEDE------SDDDNM------------------------ 255
Hsapiens_a3             EKYAKESLKEEDE------SDDDN------------------------- 254
Mmusculus_a3            EKYAKESLKEEDE------SDDDNM------------------------ 255
Dmelanogaster_a7        RKAGDAANKDEDS------DNETH------------------------- 253
Athaliana_a3            KTAAKTALEEMDA------D-------------------------- 249
Scerevisiae_Pre10       IDFAQKEINGDDDEDEDDSDNVMSSDDENAPVATNANATTDQEGDIHLE 288
Spombe_a7               EAYARRIADGEEE------DIAMQE------------------------ 253
                           .    .  :       .
```

SUPPLEMENTARY FIG. S5 (continued). Alignments were performed with the software MegAlign DNASTAR Lasergene 9 Core Suite and those of text format with the ClustalW2 - European Bioinformatics Institute (http://www.ebi.ac.uk/Tools/msa/clustalw2/). Sequences were obtained from SGD (Saccharomyces Genome Database) and NCBI Protein Database.

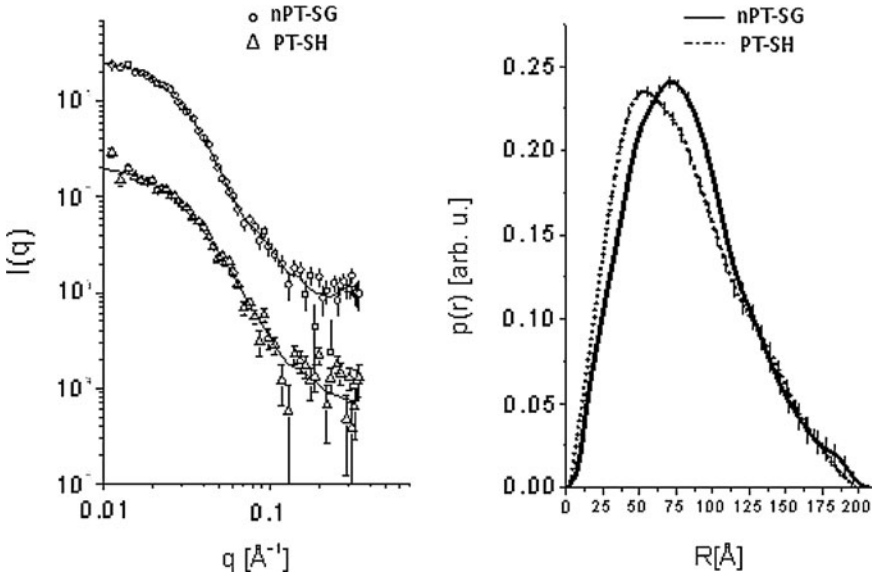

SUPPLEMENTARY FIG. S6. Model fit of the SAXS data using indirect Fourier transformation (IFT). *Left:* Experimental data; nPT-SG (circles), PT-SH (triangles), IFT fit (solid lines). The curves were split for clarity. *Right:* Pair distance distribution functions; nPT-SG (solid line), PT-SH (dotted line).

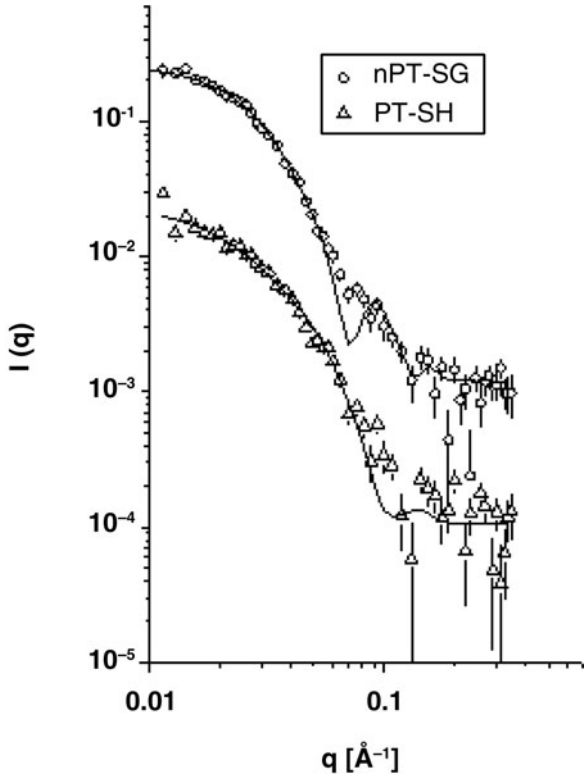

SUPPLEMENTARY FIG. S7. Model fit of the SAXS data using the cylinder form factor. *Left:* Experimental data; nPT-SG (circles), PT-SH (triangles), theoretical fit (solid lines). The curves were split for clarity.

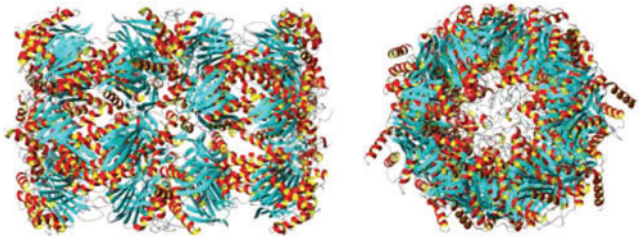

SUPPLEMENTARY FIG. S8. Representation of the structure 3d29 in two views, side and top.

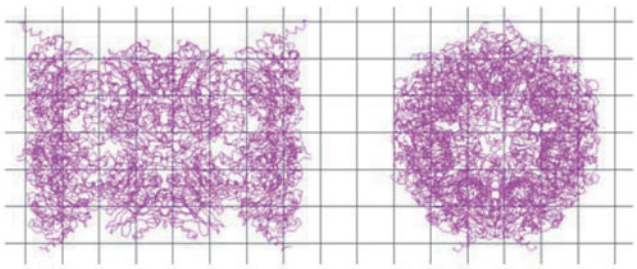

SUPPLEMENTARY FIG. S9. Representation of the structure 3d29 on a grid panel to retrieve characteristic sizes.

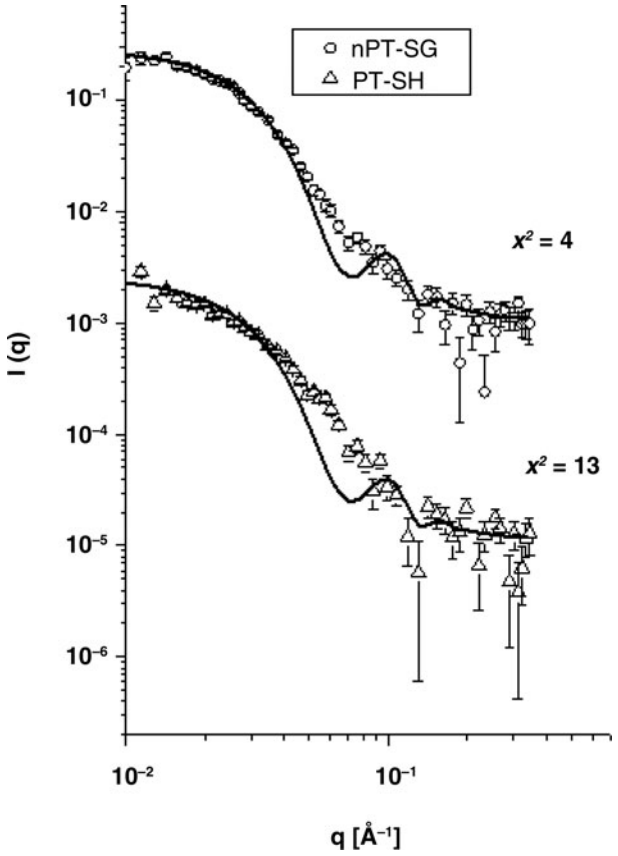

SUPPLEMENTARY FIG. S10. Fitting of the experimental data with the theoretical intensity calculated from structure 3d29.

Supplementary Table S1. 20SPT Dimensions Obtained With Different Techniques

Diameter (Å)	*Lenght (Å)*	*Pore (Å)*	*Species*	*Technique*	*Source*	*Obs*
106	188	80	*Saccharomyces cerevisiae*	SAXS	Present work	Open – nPT-SG
72	210	0–10	*S. cerevisiae*	SAXS	Present work	Closed – PT-SH
120	154	10	*S. cerevisiae*	Crystal	(3)	
nd	nd	9/20	*Termoplasma acidophilum*	Crystal	(15)	Closed/ Open
113	148	13	*T. acidophilum*	Crystal	(9)	
100–130	150–170	nd	*S. pombe*	AFM	(11)	
80–120	130–170	nd	*S. cerevisiae*	AFM	(13)	Log phase[a]
90–120	140–170	nd	*S. pombe*	AFM	(12)	Open – cylinder[b]
80–110	140–160	nd	*S. pombe*	AFM	(12)	Closed – barrel[c]
110	150	nd	*T. acidophilum*	TEM	(5)	
120	170	40	*Anas platyrhynchos*	TEM	(1)	
nd[d]	210		*S. cerevisiae*	SAXS	Present work	ΔNα3α720SPT[e]
nd[e]	230		*S. cerevisiae*	SAXS	Present work	ΔNα3α720SPT[f]

[a]Proteasome purified from yeast cells in the log phase of growth.
[b,c]Proteasomes described with cylinder and barrel shapes, respectively.
[d,e]Although no change in the diameter between analyzed samples was predicted, we did not succeed to measure the dimension.
[e]Proteasome purified from cells grown to stationary phase into YPD were treated with 20 mM DTT.
[f]Same samples incubated with 1 mM GSH.
SAXS, small angle X-ray scattering; AFM, atomic force microscopy; TEM, transmission electron microscopy; nd, not determined.

Supplementary Table S2. Identification of the 20SPT Subunits by Peptide Mass Fingerprinting

Subunit	*Protein*	*Theoretical mass (Da)*	*Theoretical pI*	*Sequence coverage (%)*	*Matched peptides*	*MOWSE score*
α1	Scl1	28,001	6.17	42	10	68
α2	Pre8	27,162	5.5	22	5	62
α3	Pre9	28,714	4.91	69	16	106
α4	Pre6	28,439	7.37	46	7	74
α5	Pup2	28,617	4.49	52	12	91
α6	Pre5	25,604	7.43	73	12	114
α7	Pre10	31,536	4.9	22	5	60
β1	Pre3	23,547	5.73	44	8	66
β2	Pup1	28,268	6.6	14	4	74
β3	Pup3	22,605	4.87	24	4	59
β4	Pre1	22,516	6.15	29	6	87
β5	Pre2	31,636	6.17	32	8	89
β6	Pre7	26,871	5.99	50	11	63
β7	Pre4	29,443	5.81	47	8	86
P1	Pnc1	24,993	6.23	40	7	107

MALDI-TOF MS analyses of proteasomal subunits isolated by 2-DE PAGE followed by digestion with trypsin were performed using an Ettan MALDI-TOF instrument (Amersham Biosciences). Probability-based MOWSE scores were obtained using Mascot Server 2.2 software (Matrix Science, UK). Scores higher than 56 were statistically significant ($p < 0.05$). In addition to the 14 proteasomal subunits, nicotinamidase Pnc1 was also identified.

Supplementary Table S3. The Redox Forms of 20SPT-Cys Residues in Preparations Obtained From Cells Grown to Stationary Phase in YPD

Cys	*Tryptic peptide sequence*	*SH*	*GSH*	*SOH*	*SO_2*
α1					
C50	GKDCTVVISQK	+ +			+
C50	DCTVVISQK	+			
C74	LLDPTTVSYIFCISR	+			
C114	YGYDMPCDVLAK	+ +			
α4					
C32[a]	GTCAVGVK	+ +			
C41	NCVVLGCER	+ +			
C46[a]	NCVVLGCER	+			
C191	KEPPATVEECVK	+ +			
α5					
C76	HIGCAMSGLTADAR	+ +	+ +		+ +
C117	TAAVTHNLYYDEDINVESLTQSVCDLALR	+ +	+		+ +
C221	QVMEEKLDENNAQLSCITK	+	+		
C221	LDENNAQLSCITK	+ +	+		+
α6					
C66	CDEHMGLSLAGLAPDAR	+ +	+		
C92	QQCNYSSLVFNR	+ +			
C113	AGHLLCDK	+			
α7					
C42	CNDGVVFAVEK	+ +	+		+ +
C76	HIGCVYSGLIPDGR	+ +	+		+
C219	DFELEISWCSLSETNGLHKFVKGD	+			
β1					
C62	IWCCR	+			
C63	IWCCR	+			
C105	ELCYENK	+			
C157	LPYAIAGSGSTFIYGYCDK	+ +			
β3[b]					
C20	DCVAIACDLR	+			+
β4[b]					
C164	LCVQELEK	+			+
C164	LCVQELEKR	+			
C219[a]	DFELEISWCSLSETNGLHKFVKGD	+			
β5					
C127[a]	VKRVIEINPFLLGTMAGGAADCQFWET	+ +			
C138[a]	VKRVIEINPFLLGTMAGGAADCQFWETWLGSQC	+ +			
C177	GAGLSMGTMICGYTR	+			
C203	LKGDIFCVGSGQTFAYGVLDSNYK	+ +			+ +
β6					
C66	YEPKVFDCGDNIVMSANGFAADGDALVK	+ +		+	+ +
C155[a]	EQCR	+ +			

All 14 proteasomal subunits were identified on the 2-DE gel, as shown in Supplementary Fig. 1S (numbered spots). Those spots containing Cys residues were digested, followed by LC-Q-ToF-MS. Subunits α2, α3, and β7 do not contain Cys. Seven Cys residues and their respective fragments distributed into β2 (C60, C62, C205, and C250) and β3 (C25, C129, and C150) subunits were not identified. Among the 35 Cys present in the mature form of the yeast 20SPT, 28 were identified in the present study. Thirty-six Cys in the 20S PT were deduced from the genomic sequence (www.yeastgenome.org). Only 35 of the 36 in the mature 20S PT were mentioned because the cleavage of the β5 subunit at G75 removes the Cys 68 (4). Other cleavages during 20S PT maturation, all reported for the β subunits, do not imply the removal of any Cys residue (4).

(+) indicates the redox state of Cys residues found in the fragments identified by LC-Q-ToF-MS analyses from tryptic fragments of samples obtained, as shown: **Red:** nPT-SG (20SPT purified from cells grown into YPD); **Green:** nPT-SG samples treated with 10 mM GSH (PT-SG). Subunits analyzed were: α1, α4, α5, α6, α7, β3, and β5. In this set of experiments, the buffers utilized for cell lysis and during the entire proteasome purification procedure contained 20 mM IAA to alkylate reduced cysteines, avoiding their oxidation during sample manipulation.

[a]These fragments were identified only in the absence of iodoacetamide (IAA).

[b]These subunits were not analyzed in nPT-SG preparations.

LC-Q-ToF-MS, liquid chromatography-quadrupole-time of flight-mass spectrometry.

Supplementary Table S4. Chymotrypsin-like Proteasomal Activity by the Redox Forms of the 20SPT

	nPT-SG	*PT-SH*
$V_{max/min}$	7.5 ± 0.5	10 ± 0.1*

20S proteasomal preparations were incubated with the *suc*-LLVY-AMC substrate, and the fluorescence emission was recorded for 45 min. The results shown are expressed as the means ± SD of V_{max}/min.

*$p \leq 0.0034$.

References

1. Coux O, Tanaka K, and Goldberg AL. Structure and functions of the 20S and 26S proteasomes. *Annu Rev Biochem* 65: 801–847, 1996.
2. Glatter O. A new method for the evaluation of small-angle scattering data. *J Appl Cryst* 10: 6, 1977.
3. Groll M, Ditzel L, Lowe J, Stock D, Bochtler M, Bartunik HD, and Huber R. Structure of 20S proteasome from yeast at 2.4 A resolution. *Nature* 386: 463–471, 1997.
4. Groll M, Heinemeyer W, Jager S, Ullrich T, Bochtler M, Wolf DH, and Huber R. The catalytic sites of 20S proteasomes and their role in subunit maturation: a mutational and crystallographic study. *Proc Natl Acad Sci U S A* 96: 10976–10983, 1999.
5. Hegerl R, Pfeifer G, Puhler G, Dahlmann B, and Baumeister W. The three-dimensional structure of proteasomes from *Thermoplasma acidophilum* as determined by electron microscopy using random conical tilting. *FEBS Lett* 283: 117–121, 1991.
6. Hines J, Groll M, Fahnestock M, and Crews CM. Proteasome inhibition by fellutamide B induces nerve growth factor synthesis. *Chem Biol* 15: 501–512, 2008.
7. Konarev PV, Petoukhov MV, and Svergun DI. MASSHA—a graphics system for rigid-body modelling of macromolecular complexes against solution scattering data. *J Appl Cryst* 34: 5, 2001.
8. Koradi R, Billeter M, and Wuthrich K. MOLMOL: a program for display and analysis of macromolecular structures. *J Mol Graph* 14: 51–55, 29–32, 1996.
9. Lowe J, Stock D, Jap B, Zwickl P, Baumeister W, and Huber R. Crystal structure of the 20S proteasome from the archaeon *T. acidophilum* at 3.4 A resolution. *Science* 268: 533–539, 1995.
10. Oliveira CL, Behrens MA, Pedersen JS, Erlacher K, and Otzen D. A SAXS study of glucagon fibrillation. *J Mol Biol* 387: 147–161, 2009.
11. Osmulski PA and Gaczynska M. Atomic force microscopy reveals two conformations of the 20 S proteasome from fission yeast. *J Biol Chem* 275: 13171–13174, 2000.
12. Osmulski PA and Gaczynska M. Nanoenzymology of the 20S proteasome: proteasomal actions are controlled by the allosteric transition. *Biochemistry* 41: 7047–7053, 2002.
13. Osmulski PA, Hochstrasser M, and Gaczynska M. A tetrahedral transition state at the active sites of the 20S proteasome is coupled to opening of the alpha-ring channel. *Structure* 17: 1137–1147, 2009.
14. Pedersen JS, Hansen S, and Bauer R. The aggregation behavior of zinc-free insulin studied by small-angle neutron scattering. *Eur Biophys J* 22: 379–389, 1994.
15. Rabl J, Smith DM, Yu Y, Chang SC, Goldberg AL, and Cheng Y. Mechanism of gate opening in the 20S proteasome by the proteasomal ATPases. *Mol Cell* 30: 360–368, 2008.
16. Svergun DI, Barberato C, and Koch, MHJ. CRYSOL—a program to evaluate x-ray solution scattering of biological macromolecules from atomic coordinates. *J Appl Cryst* 28: 5, 1995.